

Research Paper

The imaging quantification of multiple organs by dynamic ^{18}F -FDG PET/CT in discharged COVID-19 patients: A prospective pilot study

Jijin Yao, MD^{1,2#}; Jing Liu, MD^{3#}; Lei Bi, MS^{1#}; Yiying Huang, MD³; Lu Wang, MS⁴; Fanwei Zhang, MD⁵; Ying Wang, MD⁵✉ and Hongjun Jin, PhD¹✉

1. Guangdong Provincial Key Laboratory of Biomedical Imaging, Fifth Affiliated Hospital, Sun Yat-sen University, Zhuhai, Guangdong Province 519000, China.
2. Department of Head and Neck Oncology, Cancer Center, Fifth Affiliated Hospital, Sun Yat-sen University, Zhuhai, Guangdong Province 519000, China.
3. Department of Respiratory Medicine, Fifth Affiliated Hospital, Sun Yat-sen University, Zhuhai, Guangdong Province 519000, China.
4. Department of Information Technology, Fifth Affiliated Hospital, Sun Yat-sen University, Zhuhai, Guangdong Province 519000, China.
5. Department of Nuclear Medicine, Fifth Affiliated Hospital, Sun Yat-sen University, Zhuhai, Guangdong Province 519000, China.

#These authors contributed equally to this work.

✉ Corresponding authors: **Hongjun Jin, PhD**, Guangdong Provincial Key Laboratory of Biomedical Imaging, Fifth Affiliated Hospital, Sun Yat-sen University, Zhuhai, Guangdong Province 519000, China. Tel.: +86-0756-2526136; Fax: +86-0756-2523888; E-mail: jinjh3@mail.sysu.edu.cn; OR **Ying Wang, MD/PhD**, Department of Nuclear Medicine, Fifth Affiliated Hospital, Sun Yat-sen University, Zhuhai, Guangdong Province 519000, China. Tel.: +86-0756-2528032; Fax: +86-0756-2523888; E-mail: wangy9@mail.sysu.edu.cn.

© The author(s). This is an open access article distributed under the terms of the Creative Commons Attribution License (<https://creativecommons.org/licenses/by/4.0/>). See <http://ivyspring.com/terms> for full terms and conditions.

Received: 2022.04.08; Accepted: 2022.08.16; Published: 2022.09.06

Abstract

Purpose: To early identify abnormal lesions by applying the ^{18}F -FDG PET dynamic modeling approach for discharged patients recovering from COVID-19.

Methods: Seven discharged COVID-19 patients (COVID-19 group), twelve healthy volunteers (control group 1), and eight cancer patients with normal pulmonary function (control group 2) were prospectively enrolled. Control group 1 completed static ^{18}F -FDG PET/CT only; COVID-19 group and control group 2 completed 60-min dynamic ^{18}F -FDG PET/CT. Among COVID-19 group and control group 2, the uptake of FDG on the last frame (at 55–60 min) of dynamic scans was used for static analysis. Prior to performing scans, COVID-19 patients provided negative real-time Reverse Transcription-Polymerase Chain Reaction (rRT-PCR) of SARS-CoV-2, normal lung functions test, and normal laboratory test. Organ-to-liver standard uptake ratio (OLR, i.e. $\text{SUV}_{\text{max}}^{\text{evaluated organ}} / \text{SUV}_{\text{max}}^{\text{liver}}$) from conventional static data and Patlak analysis based on the dynamic modeling to calculate the ^{18}F -FDG net uptake rate constant (K_i) were performed.

Results: Compared to the control groups, COVID-19 patients at two to three months after discharge still maintained significantly higher K_i values in multiple organs (including lung, bone marrow, lymph nodes, myocardium and liver), although results for regular OLR measurements were normal for all discharged COVID-19 patients. Taking the image of lung as an example, the differences of SUV_{max} images between COVID-19 group and control group were hard to distinguish. In contrast, a high ^{18}F -FDG signal of the lung among the COVID-19 group was observed for K_i images.

Conclusion: The K_i from ^{18}F -FDG PET/CT dynamic imaging quantification might contribute to identifying residual lesions for COVID-19 survivors.

Trial registration: The trial is registered with ClinicalTrials.gov, number NCT04519255 (IRB-approved number, K52-1).

Key words: COVID-19, ^{18}F -FDG, Dynamic PET/CT, Patlak, Abnormal lesion

Introduction

The coronavirus disease 2019 (COVID-19) pandemic, caused by severe acute respiratory syndrome coronavirus 2 (SARS-CoV-2), has resulted in over 600 million confirmed cases with over 6

million deaths globally as of August 23th, 2022. During this period, more than 570 million COVID-19 patients have been discharged from hospitals worldwide. Several studies have described the long-time health

consequences of patients that recovered from COVID-19 [1, 2]; however, reliable imaging method to quantify underlying lesions for individuals that need early intervention remains not well understood. Therefore, exploring an imaging method for early identification of underlying lesions among discharged COVID-19 patients is of public health importance.

The ^{18}F -FDG PET/CT has a high sensitivity for revealing abnormal metabolic lesions utilizing a non-invasive approach [3]. This method has also been suggested to be important in detecting and monitoring inflammatory diseases [4, 5]. In addition to estimating the inflammation of lungs, ^{18}F -FDG PET/CT is beneficial for assessing metabolic and functional states for various organs throughout the body. For example, in Chefer's MERS-CoV animal model, increased bone marrow uptake over long periods were observed in follow-up ^{18}F -FDG PET/CT [6]. Therefore, ^{18}F -FDG PET/CT has the potential to reveal underlying lesions in discharged COVID-19 patients. In previous studies, the maximum standardized uptake values (SUV_{max}) have been commonly utilized for PET imaging quantification [7, 8]. Nevertheless, factors like body mass index (BMI), uptake kinetics, or post-injection time may influence SUV outcomes [9]. The absolute quantized Patlak kinetic model was used to calculate the ^{18}F -FDG net uptake rate constant (K_i) from linear modeling of graphical data [10].

To fill current gaps in knowledge, we applied the ^{18}F -FDG PET/CT dynamic modeling method, Patlak analysis, to assess imaging quantification for multiple organs among discharged COVID-19 patients. Additionally, two control groups were included to evaluate metabolic activity for each organ. The present study may provide a new direction for early identification of underlying lesions among discharged COVID-19 patients.

Methods

Participants

From February 5th to February 12th, 2020, patients discharged with COVID-19 (COVID-19 group) at our hospital were prospectively enrolled for this study. Eligible participants included: (a) diagnosis and treatment protocol for COVID-19 consistent with the World Health Organization (WHO) interim guidance [11]; (b) performing 60-min dynamic PET/CT scans two to three months following discharge; (c) negative real-time Reverse Transcription-Polymerase Chain Reaction (rRT-PCR) of SARS-CoV-2 within three days prior to performing PET/CT scans; (d) normal laboratory test and pulmonary function test before performing PET/CT scans; (e) no history of diabetes

or chronic respiratory diseases (e.g., asthma, bronchiectasis, and chronic bronchitis); and (f) complete clinical records. Overall, the COVID-19 group included seven patients that met the inclusion criteria to be enrolled in the analysis, including four cases of severe pneumonia and three of mild pneumonia. Twelve healthy volunteers (no documented record of SARS-CoV-2 infection or tumor history) who completed static PET/CT only were classified as control group 1. Another eight patients with non-metastatic, newly diagnosed thyroid cancer who completed 60-min dynamic PET/CT scans before anti-tumor therapy (e.g., surgery, radiotherapy, chemotherapy, immunotherapy, and targeted therapies) were classified as control group 2. The Research Ethics Committee of Sun Yat-sen University Cancer Center approved the study (IRB-approved number, K52-1), and written informed consent was obtained from all participants.

^{18}F -FDG PET/CT assessment

Patients were asked to fast for a minimum of six hours prior to PET/CT scans. PET/CT imaging was conducted via a 112-ring digital light guide PET/CT (uMI780, United Imaging, China) according to published guidelines for PET/CT imaging [12]. Helical CT was implemented from the head to proximal thigh prior to PET procurement based on the standardized protocol. Static acquisitions from head to proximal thigh were obtained 45 minutes post ^{18}F -FDG injection and lasted for a period of 15 minutes. Dynamic acquisitions were done as follows: imaging started at the time of injection of ^{18}F -FDG (3.75 MBq/kg produced from Guangzhou Atom High Tech Radiopharmaceutical Co.,Ltd., Guangdong Province, China) and continued for 60 minutes. Dynamic scans were conducted from the lung apex to the liver for the COVID-19 group and control group 2. Each dynamic PET study lasted 60 minutes that contained 48 frames (time \times frame: 5s \times 18, 10s \times 6, 30s \times 5, 60s \times 5, 150s \times 8, 300s \times 6) and was adjusted for isotope decay, scattering events, and random coincidence.

PET data acquisition and analysis

The ^{18}F -FDG uptake of myocardium, spinal cord, lung, bone marrow, lymph nodes, and liver were evaluated for the three study groups. To obtain the time activity curve (TAC) for the evaluated organs, ellipsoid volumes of interest (VOIs) were drawn over manually for each organ. The regions of SUV_{max} for myocardium and spinal cord were sketched as VOIs for each organ. Regarding lung, only those with suspected pulmonary abnormal lesions (i.e., patchy shadows, ground-glass opacity, and consolidated

nodule) that both radiologists have confirmed, were sketched in COVID-19 group, and the same site was drawn in the control group 2. To determine whether the bone marrow has high metabolic uptake, the regions of SUV_{max} in the sternum and rib were delineated as VOIs. The vertebrae were not included because the free fluorine-18 tends to accumulate in the vertebrae and affects the results. The visible (≥ 3 mm) mediastinal lymph nodes, para-aortic lymph nodes, and hilar lymph nodes were delineated as VOIs. If no visible lymph nodes were observed, the regions of SUV_{max} in the corresponding lymph node station were delineated. The liver dome area is susceptible to motion artifact resulting from breathing, the area 3-5 cm below the upper edge of the right lobe of the liver was delineated as VOIs.

Carimas software (<http://turkupetcentre.fi/carimas/>) published and freely distributed by the Turku PET Center was used for data and image analysis. The plugin of "Parametric image filter" from Carimas was used to generate static (SUV) and dynamic parametric (K_i) PET images. **Figure S1** described the detail steps to generate parametric image. Conversely, VOIs were drawn manually on early frames in descending aorta (DA) to obtain the image-derived input functions (IDIF) in each patient. To minimize spillover and partial volume reactions, regions were small and far from the myocardial wall [13]. These input VOIs were then projected onto all 48 frames yielding whole arterial blood TAC, (i.e., IDIF) (**Figure 1A**). The VOIs of evaluated organs were then projected on descending aorta given the dynamic study to provide TACs (**Figure 1B**). Overall, dynamic analyses for the COVID-19 group and control group 2 were performed on organs within the range single field of view. Detailed methods of the dynamic analysis were described in detail in our previous

study [14]. Additionally, the SUV_{max} of evaluated organs were determined. Among COVID-19 group and control group 2, the uptake of FDG on the last frame (at 55–60 min) of dynamic scans were used for static analysis. To reduce variation of experiments, i.e., possible inaccuracies regarding uptake kinetics, post-injection time, and BMI [15], the organ-to-liver standard uptake ratio (OLR, i.e. $SUV_{max}^{evaluated\ organ}/SUV_{max}^{liver}$) of evaluated organs was consequently calculated.

Laboratory test and pulmonary function test

Methods for laboratory confirmation of COVID-19 were previously described in detail [16]. Blood was collected from all patients to determine the presence of D-Dimer, C-reactive protein (CRP), lactate dehydrogenase (LDH), and lymphocyte (LY). Laboratory tests were performed every day during the first week after admission, and once every 1-2 days thereafter or adjusted frequency of laboratory test according to patient's medical condition. We performed lung function tests following the National Thoracic Society and European Respiratory Society (ATS-ERS) guidelines [17]. The parameters measured including forced expiratory volume in the first second (FEV1), forced vital capacity (FVC), forced expired flow at 50% of FVC (FEF₅₀), total lung capacity (TLC), residual volume (RV), carbon monoxide diffusing-capacity (DLCO), and carbon monoxide diffusing-capacity corrected for alveolar volume (DLCO/VA). All lung function values were reported as a percentage for the predicted values after adjusting for age, sex, weight, and height. The lung function test was required to be completed one month after discharge. If the test was abnormal, reexamination of lung function test is required the next month.

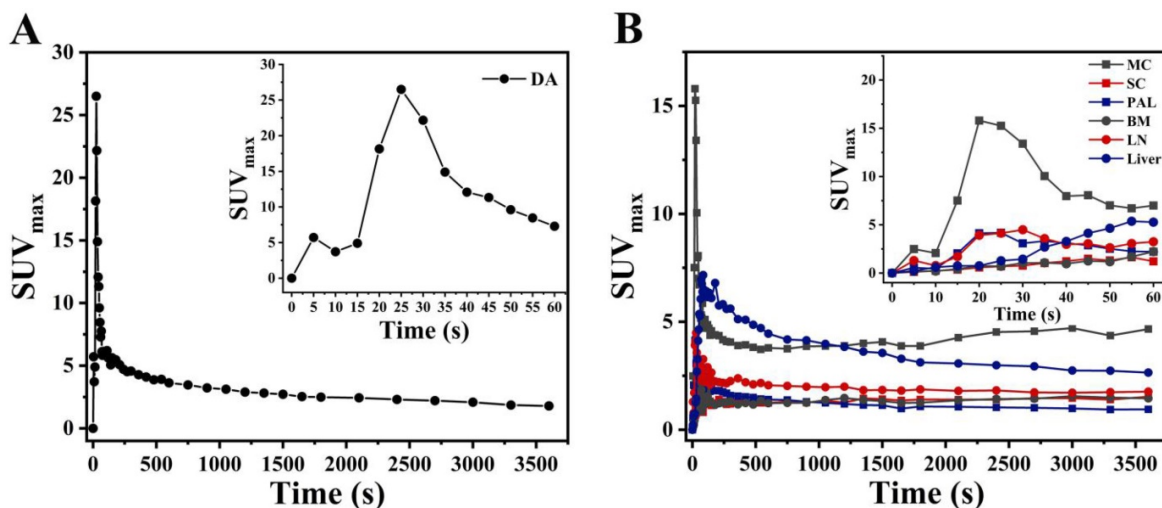


Figure 1. PET image-derived input function from a dynamic acquisition. Input function (the first 60s after injection) on descending aorta (A). Time activity curves (TAC) of myocardium (MC), spinal cord (SC), pulmonary abnormal lesions (PAL), bone marrow (BM), lymph nodes (LN), and liver from COVID-19 group.

Statistical analysis

The Statistical Package for the Social Sciences 19.0 was utilized for all analysis (Chicago, IL, USA). Clinical and demographic characteristics were obtained for each study cohort reported. Regional group differences in OLR and K_i values were compared between COVID-19 and the other two control groups using one-way non-parametric ANOVA (Kruskal-Wallis) test. A p -value < 0.05 was the threshold for statistical significance.

Results

Baseline clinical characteristics of subjects

For the COVID-19 group, the mean time and standard deviation (SD) from illness onset to admission was 5.9 (4.6) days, and the mean time to discharge was 23.7 (5.8) days. **Figure S2** presents how the examinations were performed and treatments were managed for each COVID-19 patient during the study period (i.e., given as the time from the illness onset to the day of PET/CT examination). A total of 367 laboratory tests were performed during the study period (i.e., given as the time from the illness onset to the day of last follow up). A total of 40 imaging examinations were performed, most of which were concentrated within 1-2 weeks after admission. The mean time (SD) of using antibiotic, antiviral, anti-inflammatory, and passive immunization were

14.3 days (3.6), 9.3 days (3.8), 8.4 days (2.6), and 4.1 days (1.9) respectively. Baseline demographic characteristics were compared among COVID-19 group, control group 1, and control group 2. There were no significant differences regarding the male-female ratio, BMI, age at PET scan, and years of education among the study groups ($p > 0.05$ for all; **Table 1**). In addition, chronic respiratory diseases (e.g., asthma, bronchiectasis, and chronic bronchitis) were not reported among all included patients.

Lung function recovery and laboratory recovery

At admission, the abnormal laboratory test of D-Dimer, CRP, LDH, and LY counts were observed in 4 patients (4/7), 7 patients (7/7), 5 patients (5/7), and 5 patients (5/7), respectively. **Figure S3** presents the dynamic changes of laboratory indicators across pneumonia types. Laboratory indicators tended to increase in the first week after admission, and then gradually return to normal. The mean time from admission to full recovery in laboratory test was 12.8 days (ranging 10-15 days). At one month after discharge, only one patient (Case 1) suffered a slightly impaired lung function (i.e., FVC [75.7%], DLCO [68.0%], and DLCO/VA [76.0%]) (**Table 2**). However, abnormal lung function disappeared at two months following discharge for this patient (**Table S1**).

Table 1. Comparison of demographic characteristics, OLR, and K_i values among the studied groups

Characteristics	COVID-19	Control 1	Control 2	P values ^a		
				COVID-19 vs Control 1	COVID-19 vs Control 2	Control 1 vs Control 2
Participants, No	7	12	8	0.169	0.315	0.967
Men	5	4	3	N/A	N/A	N/A
Women	2	8	5	N/A	N/A	N/A
BMI, mean (SD), kg/m ²	27.1 (2.9)	26.8 (2.7)	26.3 (2.4)	0.674	0.531	0.876
Age at PET scan, mean (SD), y	43.7 (10.2)	41.6 (8.7)	42.3 (9.3)	0.269	0.791	0.547
Years of education, mean (SD)	15.3 (2.8)	15.7 (2.3)	15.1 (2.5)	0.812	0.941	0.774
OLR of evaluated organs^b						
lung	0.143±0.036	0.108±0.025	0.110±0.024	0.271	0.314	0.946
bone marrow	0.716±0.183	0.648±0.103	0.628±0.062	0.623	0.461	0.924
lymph nodes	0.485±0.117	0.439±0.072	0.436±0.105	0.649	0.546	0.954
myocardium	1.645±0.667	1.700±0.439	1.702±0.361	0.884	0.914	0.999
spinal cord	0.533±0.169	0.493±0.076	0.481±0.104	0.674	0.416	0.931
K_i (min⁻¹) values of evaluated organs^c						
lung	0.0028±0.0011	N/A	0.0009±0.0002	N/A	<0.001	N/A
bone marrow	0.0063±0.0024	N/A	0.0032±0.0003	N/A	0.002	N/A
lymph nodes	0.0066±0.0020	N/A	0.0029±0.0013	N/A	<0.001	N/A
myocardium	0.0240±0.0089	N/A	0.0105±0.0035	N/A	0.002	N/A
spinal cord	0.0069±0.0010	N/A	0.0069±0.0013	N/A	0.969	N/A
liver	0.0077±0.0026	N/A	0.0036±0.0005	N/A	0.009	N/A

Abbreviations: OLR, organ-to-liver standard uptake ratio; BMI, Body mass index; SD, standard deviation; N/A, not applicable; COVID-19, COVID-19 survivors who completed dynamic PET/CT at two to three months after discharge; Control 1, health volunteers who completed static PET/CT; Control 2, patients with non-metastatic, newly diagnosed thyroid cancer (T1-3N0M0, based on 8th edition AJCC system) who completed both dynamic PET/CT scans before anti-tumor therapy.

^a P values are depicted for the group comparisons.

^b For static analysis, the activity concentration in evaluated organs was measured at 55–60 min after ¹⁸F-FDG injection.

^c ¹⁸F-FDG PET dynamic modeling approach, Patlak analysis, was applied to investigate the imaging quantification of lung, bone marrow, and lymph nodes.

Table 2. Pulmonary function among COVID-19 patients one month following discharge

Parameter [#]	Severe (n = 4)			Mild (n = 3)			
	Case 1	Case 2	Case 3	Case 4	Case 5	Case 6	Case 7
Spirometry							
FVC%pred, (≥80% pred)	75.70 [§]	83.00	127.90	134.90	84.60	101.20	102.70
FEV1%pred, (≥80% pred)	80.40	83.20	117.30	128.60	83.60	93.60	94.90
FEF50%pred, (≥65% pred)	113.10	75.50	90.90	90.50	87.30	73.60	68.50
Diffusion capacity							
DLCO%pred, (≥80% pred)	68.00 [§]	82.80	81.20	119.60	92.50	81.20	80.20
DLCO/VA%pred, (≥80% pred)	76.00 [§]	89.60	80.2	114.30	112.80	84.90	86.50
Lung volume							
TLC%pred, (≥80% pred)	81.80	81.40	114.80	117.00	80.70	90.50	93.70
RV%pred, (≥65% pred)	104.90	77.50	93.00	102.20	74.20	96.30	78.60

Values are presented as mean±standard deviation (SD). FVC, forced vital capacity; FEV1, forced expiratory volume in the first second; FEF₅₀, forced expired flow at 50% of FVC; DLCO, carbon monoxide diffusing-capacity; DLCO/VA, carbon monoxide diffusing-capacity corrected for alveolar volume; TLC, total lung capacity; RV, residual volume.

[#] The normal range of pulmonary parameter in each organ is indicated in parentheses.

[§] The pulmonary parameter of the organ is lower than that of the normal interval.

Pulmonary inflammation abnormal lesions

For the COVID-19 group, the mean (SD) time from discharge to the date of static ¹⁸F-FDG PET/CT examination was 59.0 (12.6) days. **Figure 2** presents the CT imaging manifestation during illness (vertical: A1-G1), follow-up CT (vertical: A2-G2), and PET/CT (vertical: A3-G3) among seven COVID-19 survivors. Of the seven patients, the first four patients (Case 1-4) suffered severe pneumonia and the last three patients (Case 5-7) suffered mild pneumonia. Case 1 showed multiple patchy and light consolidation with patchy shadows in both lungs during illness (A1; red arrows). Follow-up CT showed obvious absorption of lesions in both lungs (A2; green arrows), however, increased ¹⁸F-FDG uptake was hard to observe in both lungs. The other three severe pneumonia (Case 2-4) groups presented patchy ground-glass opacities in both lungs with patchy consolidation lesions in it (B1-D1; red arrows) during illness. The interstitial pneumonia of both lungs receded greatly in the follow-up CT, and only a small amount of grid-like thickening of interlobular septa can be seen (B2-D2; green arrows). Moreover, no increase of ¹⁸F-FDG uptake was observed (C2-D2; green arrow) among Case 2 to 4. The last three patients with mild pneumonia (Case 5-7) showed scattered ground-glass opacities during illness (E1-G1; red arrows). Only scattered interlobular septum thickenings in the follow-up CT (E2-G2; green arrow) was present, and increased ¹⁸F-FDG uptake was not observed among the mild pneumonia (E3-G3; green arrows).

Analysis of OLR values and K_i values among different groups

As presented in **Table 1**, the OLR values were compared from five organs (i.e., lung, bone marrow,

lymph nodes, myocardium, and spinal cord) among COVID-19 group, control group 1, and control group 2. Compared to control group 1 and control group 2, COVID-19 group presented with insignificant difference OLR in all evaluated organs ($p > 0.05$ for all, **Table 1**). Additionally, the values of OLR between control group 1 and control group 2 were comparable in all five organs ($p > 0.05$ for all, **Table 1**). Consistent with the result of OLR analysis, the K_i values of spinal cord ($0.0069 \pm 0.0010 \text{ min}^{-1}$ vs. $0.0069 \pm 0.0013 \text{ min}^{-1}$; $p = 0.969$) were comparable between COVID-19 group and control group 2. However, significantly higher K_i values in lung ($p < 0.001$), bone marrow ($p = 0.002$), lymph nodes ($p < 0.001$), myocardium ($p = 0.002$), and liver ($p = 0.009$) were observed in COVID-19 group compared with control 2 group (**Table 1**). Representative PET/CT images of lung and myocardium are illustrated in **Figure 3**. The differences of evaluated organs between COVID-19 group and control group 2 were hard to distinguish. There was slightly an increased ¹⁸F-FDG uptake in both posterior lung fields (white arrow) on SUV_{max} images of discharged COVID19 patients, which are not evident among the control group 2. In contrast, a high ¹⁸F-FDG signal of lung and myocardium (white arrow) from the COVID-19 group can be observed in K_i images.

Discussion

To the best of our knowledge, this is the first study to utilize dynamic ¹⁸F-FDG PET/CT for early identification of abnormal lesions among discharged patients recovering from COVID-19. Compared to the control groups, COVID-19 patients at two to three months after discharge still maintained significantly higher K_i values in multiple organs (lung, bone marrow, lymph nodes, liver, and myocardium), although results for regular SUV_{max} measurements, along with lung functions and laboratory tests were normal for all COVID-19 discharged patients. This cross-sectional study suggests that K_i from ¹⁸F-FDG PET/CT dynamic imaging quantification may provide more sensitive noninvasive method in detection of abnormal lesions among COVID-19 patients.

Recently, a follow-up for COVID-19 survivors indicated that up to 63% of patients had persistent fatigue or muscle weakness for roughly six months on average after COVID-19 [2]. Unfortunately, effective drugs to relieve the above symptoms are lacking. There are potentially multifactorial underlying mechanisms for sustained COVID-19 symptoms and may include direct effects from bone marrow abnormalities the immunological response, and corticosteroid therapy [18-20]. In our study, we

observed that K_i values of bone marrow from the COVID-19 group were significantly higher than K_i values for the control group. Consistent with the current study, Chefer et al. identified amplified ^{18}F -FDG uptake in the bone marrow post MERS-CoV infection [6]. Additionally, Dietz et al. [21] reported increased bone marrow uptake in COVID-19 patients

as well. However, we could not deduce whether increased bone marrow uptake is directly related to chronic fatigue or muscle weakness. Hence, it is necessary to further assess the relationship between bone marrow abnormality and chronic fatigue by combining the results of bone marrow interlacement for COVID-19 survivors.

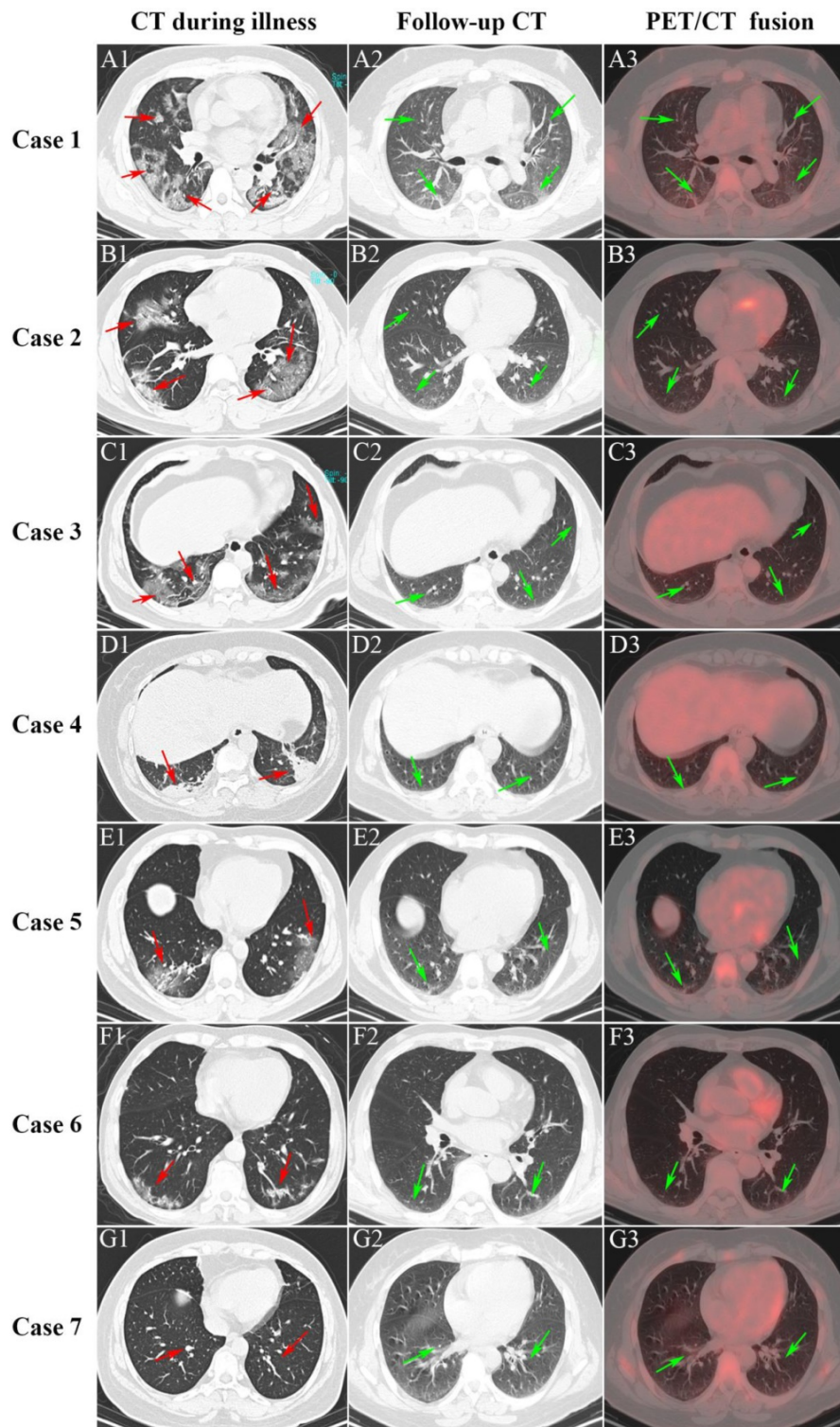


Figure 2. Serial CT and PET/CT demonstrated recovery of COVID-19. The first four patients (Case 1-4) suffered severe pneumonia and the last three patients (Case 5-7) suffered mild pneumonia.

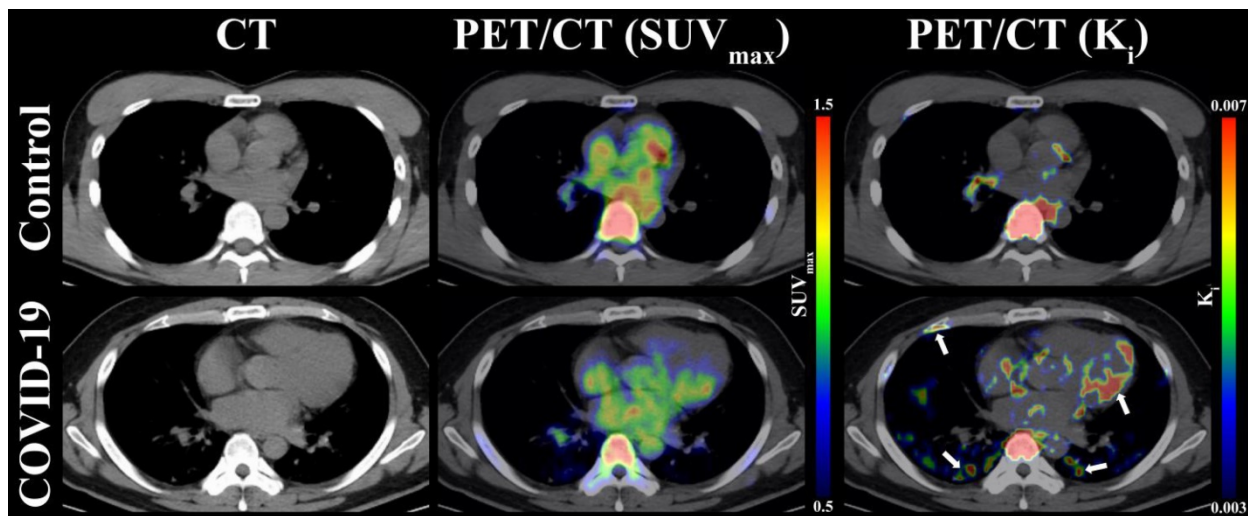


Figure 3. Representative images of lung, myocardium, and bone marrow under CT, PET(SUV_{max})/CT, and PET(K_i)/CT between COVID-19 group and control group 2. The white arrows indicate multiple abnormal lesions for COVID-19 patients at two to three months following discharge.

Literature has documented that ¹⁸F-FDG PET/CT acts as an important evaluator for inflammatory and infectious pulmonary diseases, such as COVID-19 [22]. Qin and colleagues [23] included four patients illustrating ¹⁸F-FDG PET/CT findings for individuals with acute respiratory disease produced from COVID-19 infection. They reported that three out of the four patients having multiple ¹⁸F-FDG-positive lymph nodes within the mediastinum and hilar region, and the lesions on ¹⁸F-FDG PET/CT regressed further after antiviral therapy. For SARS, autopsies suggest a large number of angiotensin 2 expression in lymph nodes and the spleen [24]. The lesions of these immune organs may be due to direct attack of the virus and indirect immune injury [25]. However, the evidence on the immune system recovery of COVID-19 survivors is minimal. In the current study, dynamic analysis observed lymph nodes in the COVID-19 group had statistically significant increases in K_i values than in the control group. This might indicate that the immune status of COVID-19 patients at two to three months after discharge is still unlike that of healthy people.

In our study, two to three months after discharge was selected as the imaging time point for PET/CT. This is due to the following two to three months after discharge is widely considered the appropriate time-point for initial assessment of recovery from pneumonia [26]. Additionally, most pneumonia would have regressed or largely resolved. As for COVID-19 progress, COVID-19 disease may damage extra-pulmonary organs, such as kidneys, heart, and other organs [26-29]. A previous study reported that COVID-19 could result in cardiac complications, including arrhythmia, heart failure, or myocardial

infarction [29]. Autopsies revealed the degeneration and focal necrosis in local cardiomyocytes [29], which was infiltrated with monocytes, lymphocytes, and neutrophils. However, it remains unclear whether COVID-19 recovered patients still have abnormal lesions in extra-pulmonary organs. Our results indicated significantly higher K_i values of the myocardium and liver in the COVID-19 group than control group 2. However, it is not possible to confirm whether there are residual lesions in the organs through histological confirmation for COVID-19 discharged patients. We therefore suggest that a consistent follow-up for those previously infected with COVID-19 is essential for understanding associations between extra-pulmonary diseases and SARS-CoV-2 infection.

Currently, SUV is widely used for quantitative evaluation of clinical ¹⁸F-FDG PET/CT examinations. However, the SUV methodology has obvious limitations, such as unsatisfactory test stability and uptake time dependence, which can adversely impact the reliability of the SUV [9, 30-31]. Compared with SUV, OLR and Patlak analysis could obviously remove some of the SUV limitations [10, 32]. We therefore selected OLR and Patlak analysis in the current study. On SUV images of discharged COVID-19 patients, a slightly increased FDG uptake in both posterior lung fields could be seen, which indicated that an SUV image may also be helpful in the detection of the abnormal focus. But no significant difference of five evaluated organs, including lung, between COVID-19 group and other two control groups were observed according to SUV. In contrast, a high ¹⁸F-FDG signal of several evaluated organs from COVID-19 group can be observed in K_i images. Moreover, K_i values of lung, bone marrow, lymph

nodes, liver and myocardium in the COVID-19 group were significantly higher than that in control group 2. This suggests K_i image provides more sensitive noninvasive method than SUV image in detection of abnormal lesions in discharged patients recovering from COVID-19.

In the current study, the significant difference of OLR in myocardium between COVID-19 group and other two control groups were not observed. These findings need to be interpreted with caution since image protocol for this study was not optimized to evaluate myocardium, which may affect the measurement of static uptake in myocardium. However, dynamic analysis was further conducted in our study, and the fasting time had little effect on the results of dynamic analysis [33]. This study was unable to obtain dynamic PET/CT for healthy volunteers, and dynamic PET/CT patients with thyroid cancer were selected for the control group, potentially impacting the results. However, dynamic PET/CT was strictly restricted for our hospital, and it is only available to patients who have received approval from an ethics committee. To reduce the impact of thyroid cancer on the results of the study, the thyroid cancer patients adopted strict inclusion criteria. They were excluded for having distant metastases, regional lymphatic metastases, and other comorbidities. We must note that the normal pre-operative evaluation does not always warrant the non-metastatic thyroid cancer after surgery or even after ^{131}I ablation. However, the static metabolic activity of evaluated organs was comparable between thyroid cancer patients and healthy volunteers, which contributed to reduce deviation within the study. Second, we were unable to collect data on pulmonary function test from two control groups since pulmonary function tests were not routinely performed in this population. Although pulmonary function tests were not performed for the control groups, patients from control groups had strict inclusion criteria, including previous fitness and no symptoms of shortness of breath, wheezing, or dyspnea. However, including pulmonary function tests would have been a more ideal measure of comparisons between patient and control groups. Finally, we failed to report the correlation analysis between the increasing K_i values and symptoms after discharge among COVID-19 survivors in the present study, due to failing to collect symptoms after discharge from COVID-19 patients. Further studies are needed to better understand this correlation.

In conclusion, we observed COVID-19 patients at two to three months following discharge continued to have a significantly higher K_i values for multiple organs, which may inspire novel concepts for

recovery of COVID-19 survivors. Compared with the regular OLR, the K_i values were more sensitive in detection of abnormal lesions among COVID-19 patients. Despite the small sample size, future longitudinal assessments in larger, less selective cohorts may provide greater insight on the causal factors associated with the health consequences for discharged hospital patients recovering from COVID-19.

Supplementary Material

Supplementary figures and tables.

<https://www.medsci.org/v19p1539s1.pdf>

Acknowledgements

The authors would like to acknowledge and thank the patients who participated in the study. Moreover, the authors appreciate Professor Chunlei Han from Turku PET Centre (Turku, Finland) for their technical support.

Funding sources

This work was funded by Zhuhai Emergence Found for COVID-19 (ZH22036302200036PWC), the National Key R&D Program of China (2018YFC0910600), the National Natural Science Foundation of China (No. 81871382, 81901699, 82150610508), the Natural Science Foundation of Guangdong, China (2021A1515220128), the program of Zhuhai Municipal Special Fund for Emergency Science and Technology Research in 2020 (ZH22036302200031PWC), Science and Technology Program of Zhuhai, China (2220004000192), and Excellent Young Researchers Program of the 5th Affiliated Hospital of SYSU (WYYXQN-2021015).

Ethics statement

Ethical approval for this research was given by the institutional review board and ethics committee of the Fifth Affiliated Hospital of Sun Yat-sen University (IRB-approved number, K52-1). All of the participants provided written informed consent.

Availability of data and materials

Datasets can be retrieved from authors upon formal request from interested readers. Datasets cannot be directly shared on public repositories due to the national personal data protection act.

Author Contributions

Authors' contributions: HJJ and YW designed the study and enrolled the patients. HJJ supervised the study. JJY, JL, LB, YYH, LW and FWZ contributed to data collection. JJY, JL, and LB performed statistical analysis. JJY, JL, and LB wrote the manuscript. HJJ and YW contributed to critical revision of the report.

All authors approved the final draft of the manuscript.

Competing Interests

The authors have declared that no competing interest exists.

References

- Xiong Q, Xu M, Li J, et al. Clinical sequelae of COVID-19 survivors in Wuhan, China: a single-centre longitudinal study. *Clin Microbiol Infect.* 2021;27(1):89-95.
- Huang C, Huang L, Wang Y, et al. 6-month consequences of COVID-19 in patients discharged from hospital: a cohort study. *Lancet.* 2021;397(10270):220-232.
- Fujii Hirofumi. [The PET, Past and Future]. *Igaku Butsuri*, 2015, 35: 2-9.
- Dell'Aquila AM, Avramovic N, Mastrobuoni S, et al. Fluorine-18 fluorodeoxyglucose positron emission tomography/computed tomography for improving diagnosis of infection in patients on CF-LVAD: longing for more 'insights'. *Eur Heart J Cardiovasc Imaging.* 2018;19(5):532-543.
- Li Y, Wang Q, Wang X, et al. Expert Consensus on clinical application of FDG PET/CT in infection and inflammation. *Ann Nucl Med.* 2020;34(5):369-376.
- Chefer S, Thomasson D, Seidel J, et al. Modeling [(18)F]-FDG lymphoid tissue kinetics to characterize nonhuman primate immune response to Middle East respiratory syndrome-coronavirus aerosol challenge. *EJNMMI Res.* 2015;5(1):65.
- Huang SC. Anatomy of SUV. Standardized uptake value. *Nucl Med Biol.* 2000;27:643-646.
- Keyes JW Jr. SUV: standard uptake or silly useless value? *J Nucl Med.* 1995;36(10):1836-1839.
- Laffon E, de Clermont H, Begueret H, et al. Assessment of dual-time-point 18F-FDG-PET imaging for pulmonary lesions. *Nucl Med Commun.* 2009;30(6):455-461.
- Patlak CS, Blasberg RG, Fenstermacher JD. Graphical evaluation of blood-to-brain transfer constants from multiple-time uptake data. *J Cereb Blood Flow Metab.* 1983;3(1):1-7.
- Clinical management of severe acute respiratory infection when COVID-19 is suspected. Released by World Health Organization on 13 March 2020. [https://www.who.int/publications-detail/clinical-management-of-severe-acute-respiratory-infection-when-novel-coronavirus-\(ncov\)-infection-is-suspected](https://www.who.int/publications-detail/clinical-management-of-severe-acute-respiratory-infection-when-novel-coronavirus-(ncov)-infection-is-suspected).
- Lv W, Yang M, Zhong H, et al. Application of Dynamic 18F-FDG PET/CT for Distinguishing Intrapulmonary Metastases from Synchronous Multiple Primary Lung Cancer. *Mol Imaging.* 2022;2022:8081299.
- Molecular Imaging 2022-06-30 | Journal article DOI: 10.1155/2022/8081299
- Yang M, Lin Z, Xu Z, et al. Influx rate constant of 18F-FDG increases in metastatic lymph nodes of non-small cell lung cancer patients. *Eur J Nucl Med Mol Imaging.* 2020;47(5):1198-1208.
- Freedman NM, Sundaram SK, Kurdziel K, et al. Comparison of SUV and Patlak slope for monitoring of cancer therapy using serial PET scans. *Eur J Nucl Med Mol Imaging.* 2003;30(1):46-53.
- Lin L, Jiang X, Zhang Z, et al. Gastrointestinal symptoms of 95 cases with SARS-CoV-2 infection. *Gut.* 2020;69(6):997-1001.
- Kharitonov S, Alving K, Barnes PJ. Exhaled and nasal nitric oxide measurements: recommendations. The European Respiratory Society Task Force. *Eur Respir J.* 1997;10(7):1683-1693.
- Mitema ES, Oehme FW, Penumarthi L, Moore WE. Effect of chronic lead exposure on the canine bone marrow. *Am J Vet Res.* 1980;41(5):682-685.
- Rusznák M, Jakó J, Francz M, Babicz T. Csontvelői myelomához társult amyloidosis által okozott obstructív cardiomyopathia [Obstructive cardiomyopathy, caused by amyloidosis, associated with bone marrow myeloma]. *Orv Hetil.* 1993;134(19):1033-1036.
- Rogers JP, Chesney E, Oliver D, et al. Psychiatric and neuropsychiatric presentations associated with severe coronavirus infections: a systematic review and meta-analysis with comparison to the COVID-19 pandemic. *Lancet Psychiatry.* 2020; 7(7):611-627.
- Dietz M, Chironi G, Claessens YE, et al. COVID-19 pneumonia: relationship between inflammation assessed by whole-body FDG PET/CT and short-term clinical outcome. *Eur J Nucl Med Mol Imaging.* 2021;48(1):260-268.
- Capitano S, Nordin AJ, Noraini AR, Rossetti C. PET/CT in nononcological lung diseases: current applications and future perspectives. *Eur Respir Rev.* 2016;25:247-258.
- Qin C, Liu F, Yen TC, Lan X. 18F-FDG PET/CT findings of COVID-19: a series of four highly suspected cases. *Eur J Nucl Med Mol Imaging.* 2020;47(5):1281-1286.
- Bradley BT, Bryan A. Emerging respiratory infections: The infectious disease pathology of SARS, MERS, pandemic influenza, and Legionella. *Semin Diagn Pathol.* 2019;36(3):152-159.
- Xiao Y, Meng Q, Yin X, et al. Pathological changes in masked palm civets experimentally infected by severe acute respiratory syndrome (SARS) coronavirus. *J Comp Pathol.* 2008;138(4):171-179.
- Chen DL, Bedient TJ, Kozłowski J, et al. [18F]fluorodeoxyglucose positron emission tomography for lung antiinflammatory response evaluation. *Am J Respir Crit Care Med.* 2009;180(6):533-539.
- Xu Z, Shi L, Wang Y, et al. Pathological findings of COVID-19 associated with acute respiratory distress syndrome. *Lancet Respir Med.* 2020;8(4):420-422.
- Yao XH, Li TY, He ZC, et al. A pathological report of three COVID-19 cases by minimal invasive autopsies. *Zhonghua Bing Li Xue Za Zhi.* 2020;49(5):411-417.
- Buja LM, Wolf DA, Zhao B, et al. The emerging spectrum of cardiopulmonary pathology of the coronavirus disease 2019 (COVID-19): Report of 3 autopsies from Houston, Texas, and review of autopsy findings from other United States cities. *Cardiovasc Pathol.* 2020;48:107233.
- Sugawara Y, Zasadny KR, Neuhoff AW, Wahl RL. Reevaluation of the standardized uptake value for fdg: variations with body weight and methods for correction. *Radiology.* 1999; 213(2):521-525.
- Hristova I, Boellaard R, Vogel W, et al. Retrospective quality control review of fdg scans in the imaging sub-study of palette eortc 62072/veg110727: a randomized, double-blind, placebo-controlled phase iii trial. *Eur J Nucl Med Mol Imaging.* 2015;42(6):848-857.
- Hofheinz F, Bütof R, Apostolova I, et al. An investigation of the relation between tumor-to-liver ratio (TLR) and tumor-to-blood standard uptake ratio (SUR) in oncological FDG PET. *EJNMMI Res.* 2016;6(1):19.
- Wu H, Dimitrakopoulou-Strauss A, Heichel TO, et al. Quantitative evaluation of skeletal tumours with dynamic FDG PET: SUV in comparison to Patlak analysis. *Eur J Nucl Med.* 2001;28(6):704-710.